Generation of acoustic waves by an impulsive point source in a fluid/solid configuration with a plane boundary

Adrianus T. de Hoop[a] and Jos H. M. T. van der Hijden
Schlumberger–Doll Research, P. O. Box 307, Ridgefield, Connecticut 06877

(Received 28 November 1983; accepted for publication 14 February 1984)

The space–time acoustic wave motion generated by an impulsive monopole point source in a fluid/solid configuration with a plane boundary is calculated with the aid of the modified Cagniard technique. The source is located in the fluid, and numerical results are presented for the reflected-wave acoustic pressure, especially in those regions of space where head-wave contributions occur. There is a marked difference in time response in the different regimes that exist for the wave speed in the fluid in relation to the different wave speeds (compressional, shear, Rayleigh) in the solid. These differences are of importance to the situation where the reflected wave in the fluid is used to determine experimentally the elastic properties of the solid.

PACS numbers: 43.20.Px, 43.20.Fn, 43.20.Bi

INTRODUCTION

Acoustic waves as a diagnostic tool in determining the mechanical parameters (volume density of mass, compressibility, elastic stiffness) of fluids and solids have a widespread use. The applications range from geophysics (seismic exploration techniques, borehole soundings) to quantitative nondestructive evaluation of mechanical structures and acoustic tomography for medical purposes. In many cases, the theoretically obtained results for certain model configurations serve as a guidance when interpreting experimentally acquired data in the more complicated situations met in practice. To serve this purpose, the relative importance of the different parameters that govern the behavior of a certain configuration should show up as clearly as possible in the results that apply to the model configuration. Now, in any acoustic wave problem where fluid/solid interfaces play a role, the case of a plane boundary between the two serves as a canonical problem whose features should be thoroughly understood before analyzing more complicated geometries.

In the present paper we investigate the acoustic wave motion in a fluid/solid configuration with a plane boundary. The source is taken to be a point source that emits an impulsive wave. In accordance with the situations met in borehole applications as well as in marine seismics, we locate the source in the fluid and compute the values of the acoustic pressure in the fluid. The corresponding problem for a two-dimensional line source has been investigated in a previous paper by the same authors.[1]

The standard approach to handle the problem is to use a Fourier transform with respect to time and a Fourier–Bessel transform with respect to the radial coordinate parallel to the boundary. For the rotationally symmetrical case the final result for the acoustic pressure is in the form of the relevant Fourier and Fourier–Bessel inversion integrals which have to be evaluated either numerically or, in certain regions of observation, asymptotically. This setup of the problem runs along the lines that are shown in Aki and Richards[2] for a two-fluid configuration. In the present paper, the problem is solved by applying the first author's modification of Cagniard's technique (de Hoop,[3,4] see also Miklowitz,[5] and Aki and Richards[6]). The answer has a fairly simple shape: just a convolution of the input signal of the source and an explicit expression, in the form of a bounded integral, for the space–time Green's function of the configuration. The space–time Green's function (or "system's response") clearly shows each feature of the time behavior of the acoustic pressure at different locations in its dependence on the mechanical parameters involved. Also, the result can serve as a check on the accuracy of the numerical procedures that are used to evaluate the inversion integrals in the standard treatment of the problem, which seems to be the only available procedure in case the materials are lossy.

I. DESCRIPTION OF THE CONFIGURATION

We investigate theoretically the pulsed acoustic wave motion in a two-media configuration with a plane interface. One of the media is a homogeneous, ideal fluid; the other is a homogeneous, isotropic, perfectly elastic solid. The source is located in the fluid. It generates an impulsive wave motion that is reflected at the interface and, in this way, interacts with the solid. We determine expressions for the acoustic pressure of the reflected wave at any point in the fluid and at any time with the aid of the modified Cagniard technique.

To specify position in the configuration, we employ Cartesian coordinates $\{x_1 = x, x_2 = y, x_3 = z\}$ with respect to a Cartesian reference frame with origin O and the three mutually perpendicular base vectors of unit length $\{\mathbf{i}_1 = \mathbf{i}_x, \mathbf{i}_2 = \mathbf{i}_y, \mathbf{i}_3 = \mathbf{i}_z\}$. In the indicated order, the base vectors form a right-handed system. The z axis is chosen normal to the interface of the two media. The source, a transmitting transducer, is located at $x = 0$, $y = 0$, $z = h_T$, with $h_T > 0$. The receiver, a receiving transducer, is located at $x = d$, $y = 0$, $z = h_R$, with $d > 0$, $h_R > 0$. The further properties of the configuration are listed in Table I (see also Fig. 1). The time coordinate is denoted by t. It is assumed that the source starts to act at the instant $t = 0$ and that prior to this instant the entire configuration is at rest.

[a] Permanent address: Delft University of Technology, Department of Electrical Engineering, Laboratory of Electromagnetic Research, P. O. Box 5031, 2600 GA Delft, The Netherlands.

 0001-4966/84/061709-07$00.80

TABLE I. Properties of the fluid/solid configuration.

	Fluid	Solid
Domain	D_f	D_s
z coordinate	$0<z<\infty$	$-\infty<z<0$
Volume density of mass	ρ_f	ρ_s
Constitutive parameter(s)	K (bulk modulus of compression)	λ, μ (Lamé coefficients)
Wave speed(s)	$c_f=(K/\rho_f)^{1/2}$	$c_P=[(\lambda+2\mu)/\rho_s]^{1/2}$ $c_S=(\mu/\rho_s)^{1/2}$

II. DESCRIPTION OF THE WAVE MOTION IN THE CONFIGURATION

In the fluid, the acoustic wave motion consists of the superposition of the incident wave and the reflected wave. The incident wave is the wave that would be generated by the transmitting transducer if the fluid were of infinite extent; it will be denoted by the superscript "i." The reflected wave is the difference between the actual wave motion in the fluid and the incident wave; it will be denoted by the superscript "r." In the fluid we consider the acoustic pressure p as the fundamental unknown quantity and hence we have

$$p=p^i+p^r \quad \text{in the domain } D_f . \tag{1}$$

The transmitted wave in the solid consists of a P wave that travels with speed c_P and whose particle displacement $\mathbf{u}^P$ is curl free, and an S wave that travels with speed c_S and whose particle displacement $\mathbf{u}^S$ is divergence free. In the solid we consider the particle displacement $\mathbf{u}$ as the fundamental unknown quantity and hence we have

$$\mathbf{u}=\mathbf{u}^P+\mathbf{u}^S \quad \text{in the domain } D_s . \tag{2}$$

In the modified Cagniard technique we first calculate the wave constituents in the transformed domain, i.e., after having carried out a one-sided Laplace transform with respect to time, with real, positive transform parameter s, and a Fourier transform with respect to the coordinates x and y that are parallel to the interface, with transform parameters $s\alpha$ and $s\beta$, respectively. To show the notation, we write down the relevant transforms for the acoustic pressure:

$$\hat{p}(x,y,z,s)=\int_0^\infty \exp(-st)p(x,y,z,t)dt , \tag{3}$$

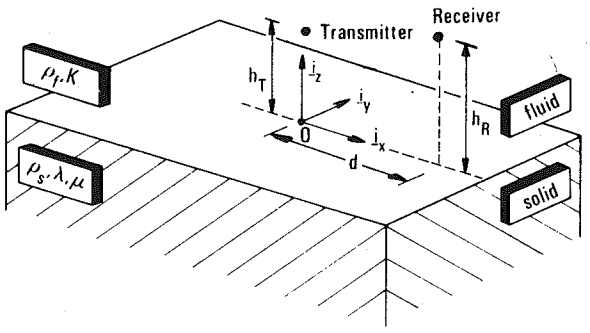

FIG. 1. Fluid/solid configuration with transmitter and receiver in fluid.

$$\tilde{p}(\alpha,\beta,z,s)=\int_{-\infty}^{\infty} dy \int_{-\infty}^{\infty} \exp[is(\alpha x+\beta y)]\hat{p}(x,y,z,s)dx, \tag{4}$$

$$\hat{p}(x,y,z,s)=\left(\frac{s}{2\pi}\right)^2 \int_{-\infty}^{\infty} d\beta \times \int_{-\infty}^{\infty} \exp[-is(\alpha x+\beta y)]\tilde{p}(\alpha,\beta,z,s)d\alpha . \tag{5}$$

In Eq. (5), we have taken into account that in Eq. (4) the transform parameters are $s\alpha$ and $s\beta$.

A. Incident wave

We now consider, more specifically, the case where the point source is a monopole source. Accordingly, we have

$$\tilde{p}^i=A^i \exp(-s\gamma_f|z-h_T|) , \tag{6}$$

where

$$\gamma_f=(1/c_f^2+\alpha^2+\beta^2)^{1/2} \quad \text{with } \mathrm{Re}(\gamma_f)\geqslant 0 , \tag{7}$$

and

$$A^i=s^2\rho_f\hat{\phi}_V/2s\gamma_f , \tag{8}$$

where $\hat{\phi}_V$ is given by

$$\hat{\phi}_V=\int_0^\infty \exp(-st)\phi_V(t)dt , \tag{9}$$

the monopole source strength being characterized by a volume density of injected fluid volume of the type

$$\Phi_V=\phi_V(t)\delta(x,y,z-h_T) . \tag{10}$$

Hence, $\phi_V(t)$ represents the pulse shape of the source signal. In the calculations we further need the z component of the particle displacement. This follows from the equation of motion and the expression Eq. (6) as

$$\tilde{u}_z^i=\pm(\gamma_f/s\rho_f)A^i \exp(-s\gamma_f|z-h_T|) \quad \text{when } z\gtrless h_T . \tag{11}$$

B. Reflected wave

For the reflected wave we write

$$\tilde{p}^r=A^r \exp[-s\gamma_f(z+h_T)] \quad \text{in the domain } D_f . \tag{12}$$

To express the linear relationship between A^r and A^i we introduce the reflection coefficient R_f for the reflected wave in the fluid through

$$A^r = R_f A^i . \tag{13}$$

The z component of the particle displacement associated with the reflected wave follows from the equation of motion and the expression Eq. (12) as

$$\tilde{u}_z^r = (\gamma_f / s\rho_f) A^r \times \exp[-s\gamma_f(z + h_T)] \quad \text{in the domain } D_f . \tag{14}$$

C. Transmitted P wave

The transform-domain representation of the transmitted P wave is written as

$$\{\tilde{u}_x^P, \tilde{u}_y^P, \tilde{u}_z^P\} = \{i\alpha, i\beta, -\gamma_P\} A^P \times \exp[s(\gamma_P z - \gamma_f h_T)] \quad \text{in the domain } D_s , \tag{15}$$

where

$$\gamma_P = (1/c_P^2 + \alpha^2 + \beta^2)^{1/2} \quad \text{with } \mathrm{Re}(\gamma_P) \geqslant 0 . \tag{16}$$

Equation (15) expresses that the P wave travels with speed c_P and that its particle displacement is curl free. In the calculations we further need the x,z, y,z, and z,z components of the stress in the solid. They follow upon substituting the expression for the particle displacement in the constitutive relation. For the P wave they follow as

$$\{\tilde{\tau}_{x,z}^P, \tilde{\tau}_{y,z}^P, \tilde{\tau}_{z,z}^P\} = 2\mu s\{i\alpha\gamma_P, i\beta\gamma_P, -(\alpha^2 + \beta^2 + 1/2c_S^2)\} \times A^P \exp[s(\gamma_P z - \gamma_f h_T)] \quad \text{in the domain } D_s . \tag{17}$$

D. Transmitted S wave

The transform-domain representation of the transmitted S wave is written as

$$\{\tilde{u}_x^S, \tilde{u}_y^S, \tilde{u}_z^S\} = \{-\gamma_S A_x^S, -\gamma_S A_y^S, -(i\alpha A_x^S + i\beta A_y^S)\} \times \exp[s(\gamma_S z - \gamma_f h_T)] \quad \text{in the domain } D_s , \tag{18}$$

where

$$\gamma_S = (1/c_S^2 + \alpha^2 + \beta^2)^{1/2} \quad \text{with } \mathrm{Re}(\gamma_S) \geqslant 0 . \tag{19}$$

Equation (18) takes into account that the S wave travels with speed c_S and that its particle displacement is divergence free. For the S wave, the x,z, y,z, and z,z components of the stress in the solid follow as

$$\{\tilde{\tau}_{x,z}^S, \tilde{\tau}_{y,z}^S, \tilde{\tau}_{z,z}^S\} = -\mu s\{(\alpha^2 + \gamma_S^2) A_x^S + \alpha\beta A_y^S, \alpha\beta A_x^S + (\beta^2 + \gamma_S^2) A_y^S, 2\gamma_S(i\alpha A_x^S + i\beta A_y^S)\} \times \exp[s(\gamma_S z - \gamma_f h_T)] \quad \text{in the domain } D_s . \tag{20}$$

With this, the transform-domain description of the wave motion in the configuration has been completed. In the next section we determine the as yet unknown amplitude coefficients A^r, A^P, A_x^S, and A_y^S by applying the boundary conditions at the fluid/solid interface.

III. DETERMINATION OF THE AMPLITUDE COEFFICIENTS OF THE REFLECTED AND TRANSMITTED WAVES

The boundary conditions at the fluid/solid interface require the continuity of the normal component of the particle displacement, the equality of the normal component of the traction in the solid and the opposite of the acoustic pressure in the fluid, and the vanishing of the tangential components of the traction in the solid. In the transform domain these conditions lead to the equations

$$\lim_{z\uparrow 0}(\tilde{u}_z^P + \tilde{u}_z^S) = \lim_{z\uparrow 0}(\tilde{u}_z^i + \tilde{u}_z^r) , \tag{21}$$

$$\lim_{z\uparrow 0}(\tilde{\tau}_{z,z}^P + \tilde{\tau}_{z,z}^S) = \lim_{z\uparrow 0}(-\tilde{p}^i - \tilde{p}^r) , \tag{22}$$

$$\lim_{z\uparrow 0}(\tilde{\tau}_{x,z}^P + \tilde{\tau}_{x,z}^S) = 0 , \tag{23}$$

$$\lim_{z\uparrow 0}(\tilde{\tau}_{y,z}^P + \tilde{\tau}_{y,z}^S) = 0 . \tag{24}$$

First, we use Eqs. (17) and (20) in Eqs. (23) and (24), and arrive at

$$A_x^S = i\alpha\gamma_P A^P / (\alpha^2 + \beta^2 + 1/2c_S^2) , \tag{25}$$

$$A_y^S = i\beta\gamma_P A^P / (\alpha^2 + \beta^2 + 1/2c_S^2) . \tag{26}$$

Next, using Eqs. (15), (17), (18), (20), (6), (11), (12), and (14) in Eqs. (21) and (22), while eliminating A_x^S and A_y^S with the aid of Eqs. (25) and (26), we arrive at

$$A^P = \frac{1}{\mu s} \frac{\alpha^2 + \beta^2 + 1/2c_S^2}{\Delta_{\mathrm{SCH}}} A^i , \tag{27}$$

$$A^r = \frac{-\rho_f\gamma_P/4\rho_s\gamma_f c_S^4 + \Delta_R}{\Delta_{\mathrm{SCH}}} A^i , \tag{28}$$

where

$$\Delta_R = (\alpha^2 + \beta^2 + 1/2c_S^2)^2 - (\alpha^2 + \beta^2)\gamma_P\gamma_S \tag{29}$$

is the "Rayleigh-wave denominator" and

$$\Delta_{\mathrm{SCH}} = \rho_f\gamma_P/4\rho_s\gamma_f c_S^4 + \Delta_R \tag{30}$$

is the "Scholte-wave denominator." The Rayleigh-wave denominator is associated with surface waves along a traction-free boundary of a solid (Rayleigh,[7] see also Achenbach[8]). The Scholte-wave denominator is associated with surface waves along a fluid/solid interface (Scholte,[9,10] see also Cagniard,[11] and Miklowitz[12]).

With this, the transform-domain expressions for the wave motion in the configuration have been fully determined. The transformation of these expressions to the space–time domain is carried out in subsequent sections. Explicit results will be given for the acoustic pressure of the reflected wave in the fluid, since in all practical applications this quantity is directly accessible to measurement.

IV. SPACE–TIME DOMAIN EXPRESSION FOR THE ACOUSTIC PRESSURE OF THE REFLECTED WAVE

Considering the fluid/solid configuration as a linear system in which, through the reflected wave, signals upon their way from the transmitting transducer to the receiving transducer gather information about the solid to be "sounded," we would like to write the time Laplace transform expression $\hat{p}^r$ for the acoustic pressure of the reflected wave as [cf. Eqs. (5), (6), (8), (12), and (28)]

$$\hat{p}^r = s^3\rho_f\hat{\phi}_V\hat{G}_f^r , \tag{31}$$

where $\hat{G}_f^r$ is the time Laplace transform of the space–time Green's function for the reflected wave in the fluid. Once the corresponding space–time Green's function G_f^r has been determined, we can write the space–time expression for the acoustic pressure p^r of the reflected wave as

$$p^r(\cdot,t)=\rho_f\partial_t^3\int_0^t \phi_V(t-\tau)G_f^r(\cdot,\tau)d\tau\,, \quad \text{when } 0<t<\infty\,. \tag{32}$$

In Eq. (32), the dot in the argument stands for the spatial variables. Now, the transform-domain equivalent of Eq. (31) would be

$$\tilde{p}^r=s^3\rho_f\hat{\phi}_V\tilde{G}_f^r\,. \tag{33}$$

Comparing Eq. (33) with Eqs. (12), (13), (28), and (8), it follows that

$$\tilde{G}_f^r=(R_f/2s^2\gamma_f)\exp[-s\gamma_f(z+h_T)]\,, \tag{34}$$

in which R_f is given by [cf. Eq. (28)]

$$R_f(\alpha,\beta)=(-\rho_f\gamma_P/4\rho_s\gamma_f c_S^4+\Delta_R)/\Delta_{\mathrm{SCH}}\,. \tag{35}$$

Starting from Eq. (34), the expression for G_f^r is obtained with the aid of the modified Cagniard technique. This technique accomplishes the transformation of the integration with respect to α and β [cf. Eq. (5)]

$$\hat{G}_f^r=\left(\frac{s}{2\pi}\right)^2\int_{-\infty}^{\infty}d\beta\int_{-\infty}^{\infty}\frac{R_f}{2s^2\gamma_f}\times\exp\{-s[i\alpha x+i\beta y+\gamma_f(z+h_T)]\}d\alpha \tag{36}$$

into the real integration

$$G_f^r(\cdot,s)=\int_T^{\infty}\exp(-s\tau)\Gamma(\cdot,\tau)d\tau\,, \tag{37}$$

where $\Gamma(\cdot,\tau)$ is an expression that does not depend on s, and where the dot stands for the spatial variables. The uniqueness theorem of the Laplace transform with real, positive transform parameter s then ensures that (Lerch's theorem, see Widder[13])

$$G_f^r(\cdot,\tau)=\begin{cases}0 & \text{when } -\infty<\tau<T,\\ \Gamma(\cdot,\tau) & \text{when } T<\tau<\infty\,.\end{cases} \tag{38}$$

Here, T apparently is the arrival time of the reflected wave. The actual transformations follow the pattern of the modified Cagniard technique for three-dimensional wave motion (see Appendix A).

The final result is obtained as

$$G_f^r(\cdot,\tau)=\begin{cases}0 & \text{when } -\infty<\tau<T_{fP}\,,\\ \displaystyle\int_0^{Q_{fP}(\tau)}\mathrm{Im}[\bar{R}_f(p^{fP},q)]\frac{1}{2\pi^2[T_{ff}^2(q)-\tau^2]^{1/2}}dq & \text{when } T_{fP}<\tau<T_{ff}\,,\\ \displaystyle\int_{Q_{ff}(\tau)}^{Q_{fP}(\tau)}\mathrm{Im}[\bar{R}_f(p^{fP},q)]\frac{1}{2\pi^2[T_{ff}^2(q)-\tau^2]^{1/2}}dq & \\ \quad\displaystyle+\int_0^{Q_{ff}(\tau)}\mathrm{Re}[\bar{R}_f(p^{ff},q)]\frac{1}{2\pi^2[\tau^2-T_{ff}^2(q)]^{1/2}}dq & \text{when } T_{ff}<\tau<T_{fP,\mathrm{end}}\,,\\ \displaystyle\int_0^{Q_{ff}(\tau)}\mathrm{Re}[\bar{R}_f(p^{ff},q)]\frac{1}{2\pi^2[\tau^2-T_{ff}^2(q)]^{1/2}}dq & \text{when } T_{fP,\mathrm{end}}<\tau<\infty\,,\end{cases} \tag{39}$$

in which the limits of the integrations are

$$Q_{fP}=\left[\left(\frac{\tau-(1/c_f^2-1/c_P^2)^{1/2}(h_T+h_R)}{d}\right)^2-\frac{1}{c_P^2}\right]^{1/2}, \tag{40}$$

and

$$Q_{ff}=\left(\frac{\tau^2}{d^2+(h_T+h_R)^2}-\frac{1}{c_f^2}\right)^{1/2}, \tag{41}$$

$$T_{fP}=\frac{d}{c_P}+\left(\frac{1}{c_f^2}-\frac{1}{c_P^2}\right)^{1/2}(h_T+h_R)\,, \tag{42}$$

is the arrival time of the head wave (if present),

$$T_{ff}=[d^2+(h_T+h_R)^2]^{1/2}/c_f \tag{43}$$

is the arrival time of the reflected body wave in the fluid,

$$T_{fP,\mathrm{end}}=\frac{d^2+(h_T+h_R)^2}{h_T+h_R}\left(\frac{1}{c_f^2}-\frac{1}{c_P^2}\right)^{1/2} \tag{44}$$

marks the end of the time interval in which the mapping Eq. (46) yields a contribution,

$$p^{ff}=\frac{d\tau+i(h_T+h_R)\{\tau^2-T_{ff}^2-[d^2+(h_T+h_R)^2]q^2\}^{1/2}}{d^2+(h_T+h_R)^2} \tag{45}$$

is the mapping from τ onto p, with q fixed, for the fluid body-wave contribution,

$$p^{fP}=\frac{d\tau-(h_T+h_R)\{[d^2+(h_T+h_R)^2]q^2+T_{ff}^2-\tau^2\}^{1/2}}{d^2+(h_T+h_R)^2} \tag{46}$$

is the mapping from τ onto p, with q fixed, for the head-wave contribution,

d = transmitter-to-receiver spacing measured along the interface,
h_T = distance from transmitter to interface,
h_R = distance from receiver to interface.

In these relations we have

$$[T_{ff}^2(q) - \tau^2]^{1/2} = [d^2 + (h_T + h_R)^2]^{1/2}(q^2 - Q_{ff}^2)^{1/2}, \tag{47}$$

$$[\tau^2 - T_{ff}^2(q)]^{1/2} = [d^2 + (h_T + h_R)^2]^{1/2}(Q_{ff}^2 - q^2)^{1/2}, \tag{48}$$

while $\bar{R}_f(p,q)$ follows from $R_f(\alpha, \beta)$ by carrying out the substitutions of Appendix A.

The head-wave contribution in Eq. (39) is only present in those regions in space where $d/[d^2 + (h_T + h_R)^2]^{1/2} > c_f/c_P$. In arriving at Eq. (39), we have assumed the case most often met in practice where $c_f < c_P$. Note, that for any solid we have $c_S < c_P$. The results hold for the two cases that remain as far as c_f is compared with c_S, viz., $c_f < c_S$, and $c_f > c_S$ ("fast formation" and "slow formation," respectively, for geoscience applications). In case $c_P < c_f$, the head-wave contribution in Eq. (39) is absent.

Finally, the integrals with respect to q in Eq. (39) are, with the aid of the transformation given in Appendix B, transformed into integrals over the fixed range $(0,\pi/2)$. The relevant transformation also removes the inverse square-root singularities that can occur at the endpoints of the q integration. After this, the integrand is smooth, and a simple numerical integration formula suffices to yield results of any desired accuracy.

V. NUMERICAL RESULTS

In this section, we present some curves showing computed space–time Green's functions. Now, the Green's function for point-source excitation does not show as many interesting features as is the case of the corresponding two-dimensional problem with line-source excitation.[1] Therefore, we shall only present results for two regimes, viz., a fast formation ($c_f < c_S$) and a slow formation ($c_S < c_f$). In Figs. 2 and 3, the space–time Green's function is plotted as a function of time for a transmitter/receiver distance $d = 0.4$ m, while $h_T = h_R = 0.01$ m.

In the case of a fast formation, numerical problems arise in the evaluation of the integral in Eq. (39) over the interval $Q_{ff} < q < Q_{fP}$. For receiver positions where a shear head wave occurs, the integrand in the relevant interval has an infinite derivative at $q = Q_{fS}$ with Q_{fS} defined by Eq. (40), with c_P replaced by c_S, an interior point of the interval for times $T_{fS} < \tau < T_{fS,\mathrm{end}}$, where T_{fS} and $T_{fS,\mathrm{end}}$ are defined by Eqs. (42) and (44) with c_P replaced by c_S. To speed up the numerical integration, we subdivide the integration interval $Q_{ff} < q < Q_{fP}$ at the point $q = Q_{fS}$, and apply the transformation of Appendix B in the two subintervals. The various regions of integration are shown in Fig. 4 and Table II. It is remarked that at $T_{fP,\mathrm{end}}$ and $T_{fS,\mathrm{end}}$ the curves in Fig. 4 do not intersect, but have a common tangent.

In Fig. 2, results are presented for a fast formation. The arrival times of the different wave types are marked by arrows. At $t = T_{fP}$, the arrival time of the compressional head wave, the Green's function has a discontinuity in slope. The jump in the slope is a finite one. At $t = T_{fS}$, the arrival time of the shear head wave, the Green's function again has a finite jump in slope. At $t = T_{ff}$, the reflected fluid-wave arrival time, the Green's function has a negative step discontinuity. Finally, at the Scholte-wave arrival time $t = T_{\mathrm{SCH}}$, defined by $T_{\mathrm{SCH}} = d/c_{\mathrm{SCH}}$, where $\Delta_{\mathrm{SCH}}(p) = 0$ at $p = \pm 1/c_{\mathrm{SCH}}$,

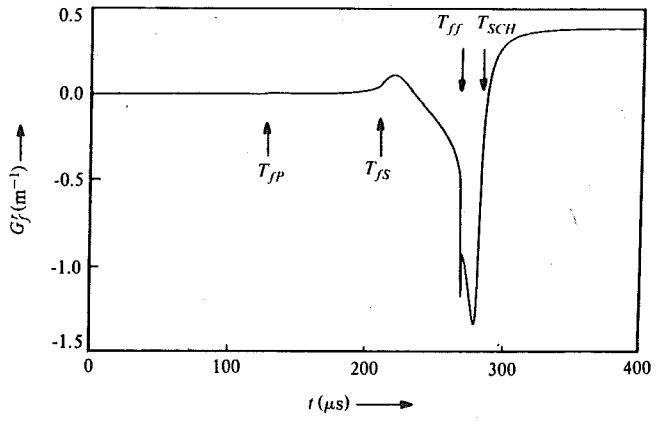

FIG. 2. Impulsive point-source space–time Green's function G_f^r for the reflected acoustic pressure in a fluid from a fluid/solid interface, as a function of time. Parameters are: $c_P = 3500$ m/s, $c_S = 2000$ m/s, $c_f = 1500$ m/s, $\rho_s/\rho_f = 2.5$, $d = 0.4$ m, and $h_T = h_R = 0.01$ m.

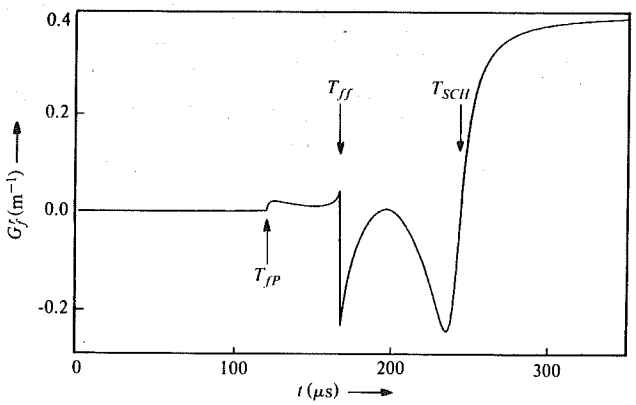

FIG. 3. Impulsive point-source space–time Green's function G_f^r for the reflected acoustic pressure in a fluid from a fluid/solid interface, as a function of time. Parameters are: $c_P = 3500$ m/s, $c_S = 2000$ m/s, $c_f = 2400$ m/s, $\rho_s/\rho_f = 2.5$, $d = 0.4$ m, and $h_T = h_R = 0.01$ m.

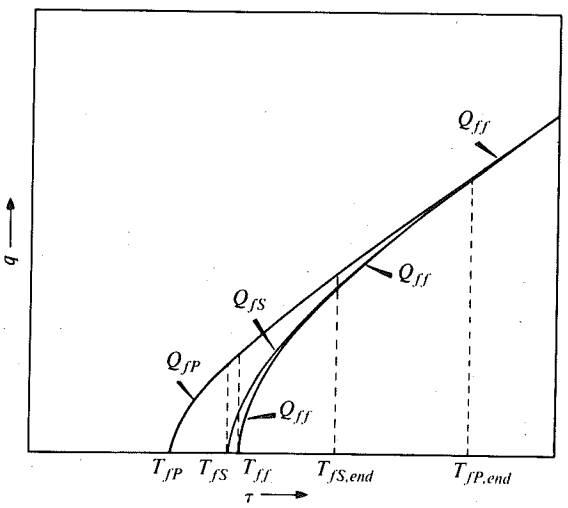

FIG. 4. Q_{fP}, Q_{fS}, and Q_{ff} as functions of τ and the various regions of integration that they define.

TABLE II. Subdivision of q integration for various τ intervals.

τ interval	q interval
$-\infty < \tau < T_{fP}$	no integration
$T_{fP} < \tau < T_{fS}$	$0 < q < Q_{fP}$
$T_{fS} < \tau < T_{ff}$	$0 < q < Q_{fS}$, $Q_{fS} < q < Q_{fP}$
$T_{ff} < \tau < T_{fS,\mathrm{end}}$	$0 < q < Q_{ff}$, $Q_{ff} < q < Q_{fS}$, $Q_{fS} < q < Q_{fP}$
$T_{fS,\mathrm{end}} < \tau < T_{fP,\mathrm{end}}$	$0 < q < Q_{ff}$, $Q_{ff} < q < Q_{fP}$
$T_{fP,\mathrm{end}} < \tau < \infty$	$0 < q < Q_{ff}$

the Green's function has a smooth fluctuation. The Green's function does not return to zero but approaches a positive final value as $\tau \to \infty$. This is consistent with the Green's function for the incident field, which is a step function in time.

In Fig. 3, the Green's function for a slow formation is shown. The major difference with the previous regime is that the shear head wave is not present anymore. Further, the Scholte wave has become less pronounced and is more separated in time from the reflected fluid-wave arrival.

In Fig. 5, we present a synthetic seismogram for the received acoustic pressure, in case the space–time Green's function has been convolved with a certain source pressure pulse. For the shape of the source pulse, we have used the second derivative of a four-point optimum Blackman window function, i.e.,

$$\rho_f \partial_t^3 \phi_V(t) = \begin{cases} 0, & \text{when } -\infty < t < 0, \\ \sum_{n=0}^{3} -b_n \left(\frac{2\pi n}{T}\right)^2 \cos\left(\frac{2\pi n t}{T}\right), & \\ & \text{when } 0 < t < T, \\ 0, & \text{when } T < t < \infty, \end{cases} \tag{49}$$

in which the constants b_n are given by $b_0 = +0.35869$, $b_1 = -0.48829$, $b_2 = +0.14128$, and $b_3 = -0.01168$, which shows great similarity with the classical Ricker wavelet often used in seismology. The time required to compute the Green's functions for one of the previous figures on a VAX 11/780 computer amounts to about 10 s.

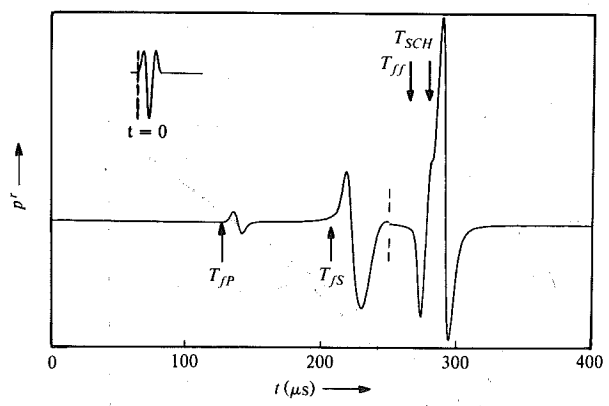

FIG. 5. Reflected acoustic pressure p^r in a fluid from a fluid/solid interface, due to an impulsive point source, as a function of time. The pressure source pulse of duration $T = 20$ μs is also shown. Further, $c_P = 3500$ m/s, $c_S = 2000$ m/s, $c_f = 1500$ m/s, $\rho_s/\rho_f = 2.5$, $d = 0.4$ m, and $h_T = h_R = 0.01$ m. The head-wave arrivals (before $t = 250$ μs) have been enlarged by a factor of 10.

VI. CONCLUSION

With aid of the modified Cagniard technique a closed-form expression has been derived for the acoustic pressure in space–time of the wave that is reflected and refracted into the fluid when an impulsive monopole point source is present near a plane interface between a fluid and a solid. Numerical results illustrate the different features that show up in the different regimes that exist for the wave speed in the fluid in relation to the wave speeds (compressional, shear, Rayleigh) in the solid. The numerical evaluation of the expressions requires much less time than would be the case for the analysis through the evaluation of the standard time–space Fourier and Fourier–Bessel inversion integrals.

APPENDIX A: TRANSFORMATIONS IN THE MODIFIED CAGNIARD TECHNIQUE

In this appendix, the main steps that lead from Eq. (36) to Eq. (37) are briefly indicated. First, the variables of integration α and β in Eq. (36) are changed into

$$\alpha = \kappa \cos(\theta) - q \sin(\theta), \tag{A1}$$

$$\beta = \kappa \sin(\theta) + q \cos(\theta), \tag{A2}$$

where θ follows from the polar-coordinate specification of the point of observation, i.e.,

$$x = r\cos(\theta), \quad y = r\sin(\theta). \tag{A3}$$

In the integration with respect to κ and q that results, q is kept real, while the integrand is continued analytically into the complex p plane, where $p = i\kappa$. For fixed q, the integration in the complex p plane is carried out along the path where

$$pr + (q^2 - p^2 + 1/c_f^2)^{1/2}(z + h_T) = \tau, \tag{A4}$$

with τ real and positive. Finally, the integrations with respect to τ and q are interchanged (see Fig. 4), which leads, together with Eq. (37), to the representation Eq. (39).

APPENDIX B: TRANSFORMATION OF THE GREEN'S FUNCTION INTEGRALS FOR NUMERICAL PURPOSES

All integrals in Eq. (39) are of the type

$$I = \int_{Q_1}^{Q_2} f(q)dq, \tag{B1}$$

with $Q_2 > Q_1$, where $f(q)$ can have inverse square-root singularities at either $q = Q_1$ or $q = Q_2$, or both. We introduce instead of q the variable of integration ψ through

$$q^2 = Q_1^2 \cos^2(\psi) + Q_2^2 \sin^2(\psi). \tag{B2}$$

Then, the interval $Q_1 < q < Q_2$, where Q_1 and/or Q_2 depend on the position of observation and on time, is mapped onto the fixed interval $0 < \psi < \pi/2$, while

$$dq = \frac{2(Q_2^2 - Q_1^2)\sin(\psi)\cos(\psi)}{[Q_1^2 \cos^2(\psi) + Q_2^2 \sin^2(\psi)]^{1/2}} d\psi, \tag{B3}$$

$$(q^2 - Q_1^2)^{1/2} = (Q_2^2 - Q_1^2)^{1/2} \sin(\psi), \tag{B4}$$

$$(Q_2^2 - q^2)^{1/2} = (Q_2^2 - Q_1^2)^{1/2} \cos(\psi). \tag{B5}$$

[1]A. T. de Hoop and J. H. M. T. van der Hijden, "Generation of acoustic waves by an impulsive line source in a fluid/solid configuration with a plane boundary," J. Acoust. Soc. Am. **74**, 333–342 (1983).
[2]K. Aki and P. G. Richards, *Quantitative Seismology* (Freeman, San Francisco, 1980), p. 200.
[3]A. T. de Hoop, "A modification of Cagniard's method for solving seismic pulse problems," Appl. Sci. Res. Sec. B **8**, 349–356 (1960).
[4]A. T. de Hoop, "Theoretical determination of the surface motion of a uniform elastic half-space produced by a dilatational, impulsive, point source," Proc. Colloq. Int. C.N.R.S. Marseille, No. 111, 21–32 (1961) (in English).
[5]J. Miklowitz, *The Theory of Elastic Waves and Waveguides* (North-Holland, Amsterdam, 1978), p. 302.
[6]R. Aki and P. G. Richards, *Quantitative Seismology* (Freeman, San Francisco, 1980), p. 224.
[7]Lord Rayleigh, Proc. London Math. Soc. **17**, 4–11 (1887).
[8]J. D. Achenbach, *Wave Propagation in Elastic Solids* (North-Holland, Amsterdam, 1973), p. 187.
[9]J. G. Scholte, "On the large displacements commonly regarded as caused by Love waves and similar dispersive surface waves," Proc. K. Ned. Akad. Wet. **51**, 533–543, 642–649, 828–835, 969–976 (1948) (in English).
[10]J. G. Scholte, "On true and pseudo Rayleigh waves," Proc. K. Ned. Akad. Wet. **52**, 652–653 (1949) (in English).
[11]L. Cagniard, *Reflection and Refraction of Progressive Seismic Waves* (McGraw-Hill, New York, 1962), p. 245. [Translation and revision of L. Cagniard, *Réflexion et Réfraction des Ondes Séismiques Progressives* (Gauthier-Villars, Paris, 1939), by E. A. Flinn and C. H. Dix.]
[12]J. Miklowitz, *The Theory of Elastic Waves and Waveguides* (North-Holland, Amsterdam, 1978), p. 168.
[13]D. V. Widder, *The Laplace Transform* (Princeton U.P., Princeton, NJ, 1946), p. 63.